Modified Sagnac interferometer for contact-free length measurement of a direct absorption cell

Hadj Elandaloussi, Christian Rouillé, Patrick Marie-Jeanne, Christof Janssen

Modified Sagnac interferometer for contact-free length measurement of a direct absorption cell

HADJ ELANDALOUSSI[1], CHRISTIAN ROUILLÉ[1], PATRICK MARIE-JEANNE[1], AND CHRISTOF JANSSEN[1,*]

[1] LERMA-IPSL, Sorbonne Universités, UPMC Univ. Paris 06, CNRS, Observatoire de Paris, PSL Research University, F-75005 Paris, France
[*] Corresponding author: christof.janssen@upmc.fr

Compiled May 2, 2016

Accurate path length measurements in absorption cells are recurrent requirements in quantitative molecular absorption spectroscopy. A new twin path laser interferometer for length measurements in a simple direct path absorption geometry is presented, along with a full uncertainty budget. The path in an absorption cell is determined by measuring the optical path length change due to the diminution of the refractive index when the cell originally filled with nitrogen gas is evacuated. The performance of the instrument based on a stabilized HeNe laser is verified by comparison with the results of direct mechanical length measurements of a roughly 45 mm long, specially designed absorption cell. Due to a resolution of about 1/300 of a HeNe fringe, an expanded (coverage factor k = 2) uncertainty of 16 µm in the length measurement is achieved, providing an expanded relative uncertainty of $3.6 \cdot 10^{-4}$ for the length of our test absorption cell. This value is about eight times lower than what has been reported previously. The instrument will be useful for precision measurements of absorption cross sections of strong absorbers which require short light paths, such as ozone, halogen oxides, sulfur dioxide and volatile organic compounds in the UV.

OCIS codes: *(120.0120) Instrumentation, measurement and metrology; (120.3180) Interferometry; (120.3940) Metrology; (120.5050) Phase measurement; (120.5710) Refraction; (140.1340) Atomic gas lasers.*

http://dx.doi.org/10.1364/ao.XX.XXXXXX

1. INTRODUCTION

Refractometers are sensitive instruments for the measurement of the dielectric properties of gases [1–4], but if the refractive indices of substances are already known the same instrumentation can be used to determine gas related quantities such as cavity lengths, gas densities or leak rates [5–8], for example. Refractrometrically based measurements of optical paths are particularly interesting, because a high accuracy is crucial for absolute trace gas measurements based on optical absorption and also because absorption cells can be integrated within current refractometer setups. The measurement method is based on measuring the variation of the refractive index during evacuation of a filled gas cell (or during filling of an evacuated cell with a gas) and the measurements often rely on interferometers which make use of accurate fringe counting [5, 6]. The interferometer configurations commonly utilized for these type of measurements are based on Michelson or Mach-Zehnder geometries with typical counting precision on the order of 1/2 [5] or 1/8 [6] of a HeNe fringe. Here, we report on a design inspired by the Sagnac geometry [9], which provides improved stability even under non-vacuum conditions. We achieve a fringe counting uncertainty of about 1/300. This is especially interesting for accurate optical path length measurements on short path cells (∼1 to 10 cm), where high accuracy on absorption measurements with low relative standard uncertainties $u_r(L)$ of 10^{-3} or less are searched for. The validity of our approach is demonstrated by direct comparison with a mechanical measurement that has been performed on a specially designed cell ($L \simeq 45$ mm), which allowed for applying both types of measurement methods. Other advantages of the interferometric technique are its contact free measurement principle, which—unlike a mechanical measurement—does not degrade the optical windows of the cell and probes directly on the cell's interior dimensions.

The paper is structured as follows. First, we describe the setup and the measurement method (Section 2). In Section 3, we then discuss measurement uncertainties following the *Guide to the expression of uncertainty in measurement* (GUM) [10]. Section 4 presents the measurement results and compares them to an independent measurement using a mechanical system. Conclusions and outlook are finally provided in the last Section 5.

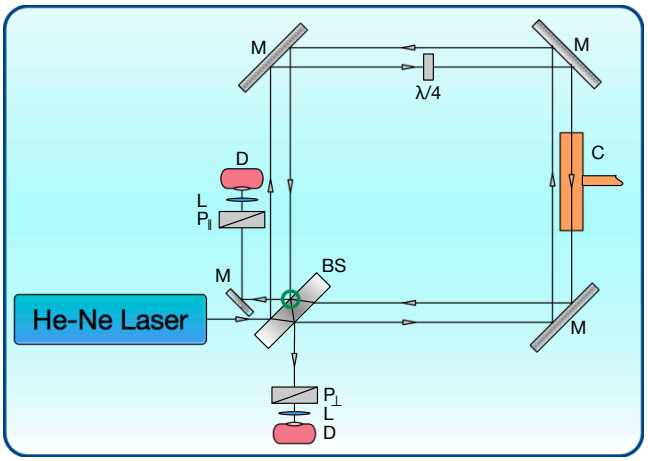

Fig. 1. (Color online) Top view on interferometer setup. L − focusing lenses, P − polarizers in ∥ or ⊥ orientation, M − plane mirrors, BS − beam splitter, D − detectors, $\lambda/4$ − quarter wave plate, C − gas cell. Light paths are indicated by straight lines with arrows indicating the direction of propagation. The interference zone at the beam splitter (BS) is indicated by a small green circle.

2. EXPERIMENTAL

A. Optical Setup and Measurement Principle

The instrument is inspired by the Sagnac interferometer configuration [9] which is operated using a 633 nm HeNe laser with a nominal relative frequency stability of $\sim 10^{-9}$. Figure 1 shows the experimental setup.

The HeNe beam is divided into two by means of a beam splitter. The two beams then travel a rectangular path in opposite directions before they recombine and interfere, again on the beam splitter. In the original Sagnac configuration, the two counter-propagating beams are superimposed. Here they are slightly separated. This permits to equipping one of the two paths with a gas cell, while still the same optical elements are used for both paths. This arrangement minimizes the impact of acoustic noise, stratification of the refractory index and of temperature effects on the interference.

The incident laser beam is linearly polarized at 45° with respect to the horizontal plane. It can thus be considered as the superposition of two perpendicularly polarized waves with polarizations in the horizontal and vertical planes, respectively denoted by $P_{\|}$ and $P_{\perp}$. A $\lambda/4$-wave plate inserted into the reference path and reflection from optical surfaces contribute to a total phase shift of $\pi/2$ between the two beams. This leads to the two interferogram signals, sine ($I_{\sin}$) and cosine ($I_{\cos}$). The path length difference between the two beams is almost zero, if the empty absorption cell is inserted into the measurement path. The two interferograms $I_{\sin}$ and $I_{\cos}$ can be expressed as a function of the phase θ due to the optical path difference in the interferometer

$$I_{\cos} = I_0(1 + V\cos(\theta)) \quad (1)$$

$$I_{\sin} = I_0(1 + V\sin(\theta)) \quad (2)$$

Here, I_0 is the intensity of the laser beam and V the contrast, which is 1 in our case. The sine and cosine interferograms are detected separately by placing filters corresponding to the two polarization directions in front of the two detectors. Signals are sampled by a NI 6251 multi purpose data acquisition card (Nat. Instr.) and treated on a PC using a LabView program (Nat. Instr.). Pressure and temperature data are acquired via RS232 interfaces and analyzed using the LabView software. The pressure is measured with a high precision gage (Mensor 6100, range 150 kPa), whose calibration (T-03231) by an accredited calibration service (DAkkS-DKD) is traceable to international metrology standards. Two Pt100 temperature probes have been installed in the cell and are connected to a data-logger (Pt-104, Picotech Inc.). Probes and data-logger were calibrated by an in-house comparison with a traceable standard platinum reference thermometer (SPRT-5626, Hart Scientific) coupled to a readout unit (1502A, Hart Scientific).

The length measurement is based on the optical path difference equation which leads to

$$L = \frac{F\lambda}{n-1}\cos\phi, \quad (3)$$

where n is the refractive index of the filled cell volume, λ the laser wavelength and $F = k + e$ the total fringe number, often represented as a sum of an integer (k) and a fractional value (e) [11]. The additional factor $\cos\phi$ takes into account the prolongation of the optical light path when the cell center axis is inclined by an angle ϕ with respect to the interferometer beam.

We determine F by calculating the phase difference $\Delta\theta$ from the initial (θ_1) and final (θ_2) phase angles, see Fig. 2. The phase

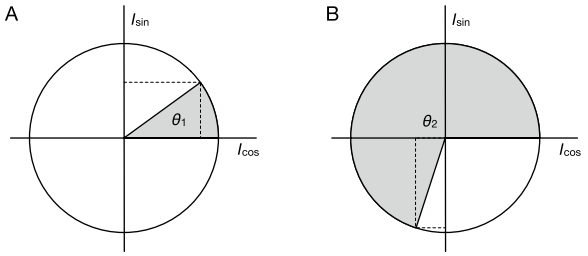

Fig. 2. Principle of phase shift measurement for fringe counting. Measurements before (A) and after (B) evacuating the cell. θ_1 is measured with respect to the $I_{\cos}$ axis, θ_2 is shown up to the k full revolutions ($2\pi k$) that have been counted using the half-fringe counter (see text).

acquired by evacuating the cell is given by

$$\Delta\theta = \theta_2 - \theta_1 = 2\pi k + \Theta, \quad (4)$$

with unique $\Theta \in [0, 2\pi[$ and integer $k \geq 0$. Using a half-fringe counter, that is incremented whenever $\sin(\theta)$ undergoes a sign change and determining initial and final phase angles by inverting

$$\tan\theta = \frac{I_{\sin}/I_0 - 1}{I_{\cos}/I_0 - 1}, \quad (5)$$

we determine the number of full circles, or fringes, k and its fraction $e = \Theta/(2\pi)$. When the cell pressure at room temperature is reduced from about 1.15×10^5 to below 10^{-2} Pa, the refractive index in the absorption cell changes by roughly $3.1 \cdot 10^{-4}$. This corresponds to $k \simeq 22$ at $\lambda \simeq 633$ nm and $L \simeq 45$ mm.

Using the experimental value for the molecular refractivity of nitrogen $\mathcal{R}' = 7.38234 \cdot 10^{-30}\,\mathrm{m}^3$ [12], which has been determined as average of five measurements under near standard ambient conditions with T between 14.6 and 19.5°C and

$p \simeq 100\,\mathrm{kPa}$, the refractive index n is found by solving the Lorentz-Lorenz or Clausius-Mosotti equation

$$\rho\mathcal{R} = \rho\mathcal{R}' N_\mathrm{A} = \frac{n^2-1}{n^2+2}, \tag{6}$$

where $\mathcal{R}$, n and ρ are the molar refractivity, the refractive index, and the molar gas density, respectively and where $N_A = 6.022140857 \cdot 10^{23}$ is the Avogadro number. The molar density of the nitrogen gas ρ is given by the measured quantities temperature and pressure via the equation of state. Within the temperature range from 270 to 350 K and at pressures below 30 MPa, the reference equation of state for nitrogen can be described by [13]

$$p = \rho RT\left(1 + \sum_{k=1}^{10} i_k N_k \delta^{i_k} \tau^{-j_k}\right), \tag{7}$$

where R is the molar gas constant, i_k, j_k and N_k are tabulated coefficients [13], and $\delta = \rho/\rho_c$ and $\tau = T/T_c$ respectively are reduced density and temperature. Here we adjusted equation (7) with respect to the original publication in order to define τ as reduced temperature rather than its inverse. We numerically invert equation (7). The relative uncertainty $u_r(\rho)$ in the gas density is smaller than 10^{-4} for pressures $p < 10\,\mathrm{MPa}$ [13]. We also note that we have employed the actually recommended value for the molar gas constant $R = 8.3144598\,\mathrm{J\,mol^{-1}\,K^{-1}}$, which deviates by 6 parts in 10^6 from the value used in the original paper. However, the nitrogen refractory index obtained from equations (6) and (7) using the results from Birch [12] and Span *et al.* [13] with these modifications yields $n - 1 = 28212.8 \cdot 10^{-8}$ at 101325 Pa and 15 °C. This is insignificantly different from the value $n - 1 = (28212 \pm 5) \cdot 10^{-8}$, reported for these conditions [12]. It also yields $n - 1 = 27367.6 \cdot 10^{-8}$ at 100 kPa and 20 °C, which is in excellent agreement with the more recent measurement of Egan and Stone [2] that gave $n - 1 = (27368.2 \pm 0.9) \cdot 10^{-8}$ under the same conditions. At 100.0000 kPa and 302.9190 K we obtain $n - 1 = 26482.73 \cdot 10^{-8}$, which agrees very well with the most recent and accurate value of $n - 1 = (26485.28 \pm 0.3) \cdot 10^{-8}$ obtained using a Fabry-Perot cavity refractometer [4]. Thus, these modified data with the uncertainty estimate by Birch [12] represent well recent results on the refractory index of nitrogen under near normal conditions with a rather conservative uncertainty value.

The vacuum wavelength of our HeNe laser has been determined using a precision wavelength meter (WS7, HighFinesse) to be $\lambda = 632.991981\,\mathrm{nm}$. The uncertainty of that value is dominated by the instrumental accuracy. The specified value of $\pm 60\,\mathrm{MHz}$ has been verified by comparing the measurement with the known emission of a reference laser (778 nm) at Laboratoire Kastler-Brossel (LKB).

B. Gas Cell and Vacuum System

The cell, which is depicted in Fig. 3 is made from a hollow inox cylinder with length of about 45 mm and 15 mm inner diameter. At the center, the outer diameter is 40 mm, but towards the two cell ends the outside diameter has been reduced in order to accommodate a thread with a 30 mm outer diameter. The two polished cell ends are closed by two N-BK7 windows of 4 mm thickness each. The windows are anti-reflection coated at 633 nm and vacuum tightness is achieved by Viton o-rings that are recessed into the cell body's faces. The cells outer threads receive brass screw caps which keep the windows in place and tightly press them against the end faces using flat o-rings made out of Teflon. The gas inlet is provided by a 10 mm outer diameter metal tube, which is soldered onto the cylindrical body and equipped with a CF flange. The flange connects to a high-voltage adapter made from ceramics which is closed up by an all-metal bellow sealed valve (type SS-8BG Swagelok/Nupro), through which cell filling and evacuation occurs. The ceramics adapter minimizes heat flow from the gas handling and vacuum system into the gas cell. Two in-house calibrated four wire Pt 100 sensors are integrated into the cell body on opposite positions for temperature measurement. Two additional thin film Pt 100 sensors are attached to the inlet tubing of the cell in order to determine thermal gradients in the inlet system.

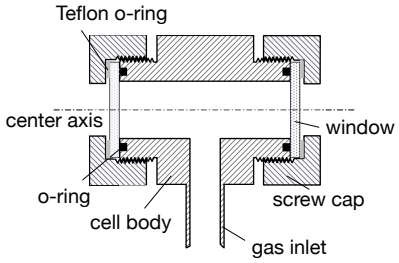

Fig. 3. Horizontal section through the inox gas cell at center height (top view). The 45 mm long cell body has a 15 mm free inner diameter. Plane end faces are polished for mechanical measurement and for well defined positioning of cell windows, which are held in place by metal screw caps. Viton o-rings are indicated by black circles and flat Teflon o-rings by grey rectangles. Temperature sensors integrated into the cell body are not shown.

The length of the cell body has been determined using a high precision linear height gage (LH600D, Mitutoyo), whose accuracy in the 40 to 50 mm range has been verified using the corresponding grade 1 gage blocks. The mechanically determined cell length was $L_1 = 44.8115\,\mathrm{mm}$ with an associated standard uncertainty $u(L_1) = 3.8\,\mu\mathrm{m}$. The latter has been determined from the repeatability ($\pm 1.0\,\mu\mathrm{m}$) of gage block measurements, from the manufacturer specified accuracy (0.7 µm), and from the observed variability ($1\sigma = 12.5\,\mu\mathrm{m}$) of 12 length measurements at different positions around the cell perimeter. The result is consistent with another length measurement at the center position, where one cell face was positioned on the measurement table, a 8.088 mm gage block was placed on top of the opposite cell face and the overall height was measured and then the gage thickness was subtracted. The result of this measurement gave $L_2 = 44.8155 \pm 0.0036\,\mathrm{mm}$. We obtain the average value $L_m = 44.8135\,\mathrm{mm}$ with an expanded ($k = 2$) standard uncertainty of $u(L_m) = 5.4\,\mu\mathrm{m}$ as the result for the mechanically determined cell length.

The gas cell is connected to a high vacuum (HV) manifold made from standard stainless steel vacuum components with copper (CF) or metal (VCR) gasket seals. The manifold connects to an ACT 200T turbopump (Alcatel) with final pressure below 1 mPa. The vacuum system can be separated from the pump via an all-metal bellow sealed valve (type SS-8BG Swagelok/Nupro). The manifold further connects to the nitrogen supply line and to the precision pressure sensor (Mensor CPT6100, 150 kPa range) with 0.01 % full scale accuracy. Nitrogen gas was used for reasons of availability and because its thermodynamic properties [13] and the refractive index [2, 4, 12] are very well known. The gas (ALPHAGAZ 1, Air Liquide) has research grade purity

(5.0), with water, oxygen and hydrocarbon (C_nH_m) impurities at mole fractions of less than 3, 0.5 and 2 μmol/mol, respectively. No attempt was made to purify the gas any further. The gas inlet to the manifold is provided by an all stainless steel bellow sealed ultra-high vacuum regulating valve (type SS-4BRG Swagelok/Nupro) equipped with VCR fittings. The valve directly connects to the two stage manometer of the gas bottle via flexible tubing (Dekabon Synflex) using Swagelok tube fittings.

C. Measurement Protocol

Experiments, which consisted out of about 20 individual runs each, were performed at four different days within two weeks using two different configurations. For the first two and for the fourth measurement series, the cell windows were aligned perpendicularly to the laser beam. In the third measurement, the cell was slightly inclined by an angle of $\phi = 2.73^\circ$ with respect to the laser.

A single measurement run consists out of four phases. In the first phase, the empty cell is slowly filled with nitrogen gas by slightly opening the valve connecting to the gas supply while keeping the pump disconnected from the vacuum manifold. The fill pressure is not regulated, but corresponds to the overpressure in the gas supply line constantly maintained by the pressure reducer. The gas supply is then shut off and the gas is allowed to accomodate all over the cell and manifold volume for about 5 minutes. In the second phase, the valve between cell and manifold is almost closed and the initial phase angle θ_1 along with temperature and pressure is continously acquired for about 20 s. In the third phase, valves connecting to the cell and the pump are opened and the system is pumped for about 20 to 30 s. Within this period the locally recorded pressure in the manifold falls to the zero value and the half-fringes are counted continuously. Then, the fourth phase begins and temperature, pressure and the final phase angle θ_2 are acquired over another 20 s period while still evacuating the system. The pumping continues for a few more minutes before a new run is started.

3. UNCERTAINTY BUDGET

The relative standard uncertainty $u_r(L)$ can be expressed as

$$u_r^2(L) = u_r^2(\lambda) + u_r^2(F) + u_r^2(\cos\phi) + u_r^2(n-1). \quad \textbf{(8)}$$

The fringe number F and the vacuum wavelength λ are directly measured quantities and the corresponding uncertainties are discussed further below.

The inclination angle ϕ is essentially zero. Only for one measurement a non-zero angle $\phi = 2.73^\circ$ has been selected. ϕ has been determined by comparing the loci of the incident and weakly reflected beams at some distance from the window. From $\tan\phi = x = d/(2l)$, where d is the displacement of the reflected from the incident beam at the front window distance $l = 157.2$ mm, one obtains

$$\cos\phi(x) = 1 \Big/ \sqrt{1+x^2}\,. \quad \textbf{(9)}$$

For non-zero ϕ, we can apply standard propagation rules and it suffices to keep just the first order terms. But the partial derivative of $\cos\phi$ with respect to x vanishes at $\phi = 0$, rendering the function strongly non-linear at this point. In line with GUM, we need considering higher-order terms in the Taylor expansion, leading to

$$u_r^2(\cos\phi) = d^2\,\frac{u^2(d) + d^2u_r^2(l)}{(d^2+4l^2)^2} + \frac{1}{2}\left(\frac{u(d)}{2l}\right)^4, \quad \textbf{(10)}$$

when we keep higher-order terms only in the vicinity of $d = 0$.

The refractive index difference between nitrogen and vacuum, $n-1$, is determined from the Lorentz-Lorenz equation (6) using the real gas equation of state (7). Under normal conditions both, the compressibility of nitrogen $Z = p/(\rho RT)$ and the factor $(2/3)(n^2+2)/(n+1)$ deviate not more than 3 parts in 10^4 from unity, so that we can base our uncertainty analysis on the simplified expression for $n-1$:

$$n - 1 \simeq \frac{3}{2}\,\frac{p}{RT}\mathcal{R}'N_\mathrm{A}. \quad \textbf{(11)}$$

This gives the straightforward expression for the relative standard uncertainty of $n-1$ in Eq. (8) in terms of the measurement quantities

$$u_r^2(n-1) = u_r^2(p) + u_r^2(T) + u_r^2(\mathcal{R}') + u_r^2(R) + u_r^2(N_\mathrm{A}). \quad \textbf{(12)}$$

Equations (8), (10) and (12) thus determine the measurement uncertainty in terms of the directly measured contributions. These individual factors will be discussed in the following and are listed as overall budget in Table 1.

A. Wavelength λ

The uncertainty of the wavelength measurement is determined by the wavelength meter, which has a manufacturer stated uncertainty range of ±60 MHz over the entire wavelength range from 370 to 1100 nm. Assuming a rectangular probability distribution function, we calculate $u_r(\lambda) = 7.3\cdot10^{-8}$. The manufacturer specification has been verified at LKB by comparing the measured position of a diode laser stabilized to the $5S_{1/2}(F=3) - 5D_{5/2}(F=5)$ two-photon transition in ^{87}Rb at 778 nm, which is known to a much higher degree of uncertainty ($u(\nu) = 1.0$ kHz) [14]. Since the observed deviation from the reference signal of 20 MHz was within the specified range, the instrument reading of $\lambda = 632.991981$ nm for the HeNe laser wavelength and the above assigned uncertainty value $u_r(\lambda) = 7.3\cdot10^{-8}$ have been adopted without further adjustment.

B. Fringe number *F*:

The principle of the fringe number measurement is discussed in Section 2.A. In practice, such a measurement takes 60 to 70 s with 20 s of measurement of the initial phase angle θ_1, the 20 to 30 s pumping period and another 20 s of measurement of the final phase angle θ_2 (see Section II.C). According to the Allan deviation analysis in Fig. 4 the associated standard uncertainty is 0.011 for θ_1, and 0.013 for θ_2, taking the drift into account. This uncertainty component thus amounts to $u_a(\theta_2-\theta_1) = 0.017$. Systematic biases arise from a slight center offset and eccentricity of the phase circle (see Fig. 2), which have been investigated in separate measurements (not shown). The impact of neglecting the small deviation from the circular shape on the value of θ depends on the phase angle, but is always within ±1°. Assuming a rectangular distribution, the associated standard uncertainty is $u_b = 0.010$. The standard uncertainty for the phase difference $\theta_2 - \theta_1$ is thus $u(F) = (u_b^2 + u_a^2)^{1/2}/(2\pi) = 0.0031$, corresponding to a relative standard uncertainty $u_r(F) = 1.4\cdot10^{-4}$ for a typical fringe number of 22.

C. Inclination factor $\cos(\phi)$:

Using graph paper, the laser beam center can be located to within ±1 mm such that the standard uncertainty in d is given by $u(d) = \sqrt{2/3}$ mm. The uncertainty in the front window distance

No	Parameter X	Unit	Typical or Recommended Value	Rel. Standard Uncertainty $u_r(X)$
1.	Length L	mm	45	$1.8 \cdot 10^{-4}$
2.	Inclination factor[a] $\cos\phi$	1	1	$4.8 \cdot 10^{-6}$
3.	Vacuum wavelength λ	m	$633 \cdot 10^{-9}$	$7.3 \cdot 10^{-8}$
4.	Fringe number F	1	22	$1.4 \cdot 10^{-4}$
5.	Refractive index difference $n-1$	1	$31000 \cdot 10^{-8}$	$1.1 \cdot 10^{-4}$
6.	Molecular refractivity $\mathcal{R}'$	m^3	$7.38234 \cdot 10^{-30}$	$6.3 \cdot 10^{-5}$
7.	Pressure p	kPa	115	$6.5 \cdot 10^{-5}$
8.	Temperature T	K	294	$6.6 \cdot 10^{-5}$
9.	Avogadro constant N_A	mol^{-1}	$6.022140857 \cdot 10^{23}$	$1.2 \cdot 10^{-8}$
10.	Universal gas constant R	$J\,mol^{-1}\,K^{-1}$	8.3144598	$5.7 \cdot 10^{-7}$

[a] Reported values are for $\phi = 0$. Due to the much larger uncertainty, measurements at $\phi = 2.73°$ are excluded from the analysis.

Table 1. Uncertainty budget of interferometric cell length measurement

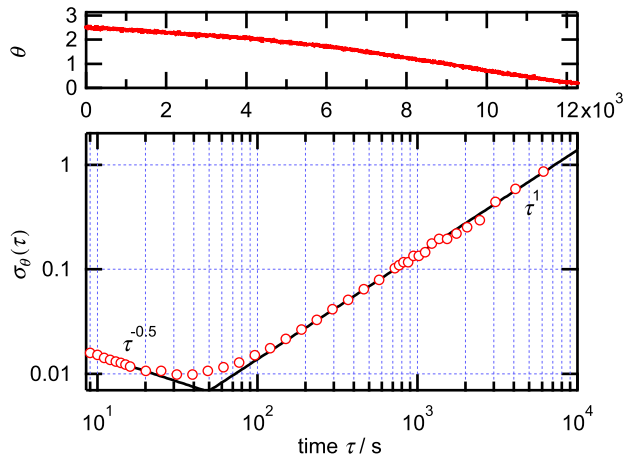

Fig. 4. (Color online) Allan deviation $\sigma_\theta(\tau)$ of the phase angle θ (circles on bottom graph) determined from a time series (line on top graph) over about 3.5 hours on an empty cell. White noise ($\propto \tau^{-0.5}$) and linear drift ($\propto \tau^1$) asymptotes are displayed as straight lines.

is estimated to be within the limits of ± 5 mm, thus yielding a standard uncertainty of $u(l) = 5/\sqrt{3}$ mm. Using Eq. (10) we derive $u_r(\cos\phi) = 1.4 \cdot 10^{-4}$ for the $\phi = 2.73°$ inclination angle. At $\phi = 0°$, we obtain $u_r(\cos\phi) = 4.8 \cdot 10^{-6}$.

D. Pressure *p*:

The pressure sensor had been manufacturer calibrated before the measurements. Readings (at 0 and 100 kPa) were confirmed to be within the guaranteed total uncertainty range ± 15 Pa ($k = 2$). During the acquisition, the reading is stable within the resolution of ± 1 Pa. At 115 kPa we derive a relative standard uncertainty $u_r(p) = 6.5 \cdot 10^{-5}$. The pressure reading at 100 kPa has further been verified to be better than 5 Pa ($5 \cdot 10^{-5}$, relative) using a calibrated barometer (Vaisala PTB210).

E. Temperature *T*:

Two cylindrical and two flat film Pt100 sensors have been calibrated in-house with respect to a reference SPRT (Hart Scientific/Fluke), which has a traceable (NPL) uncertainty of 2 mK. The absolute uncertainty of the calibration of an individual sensor is estimated at ± 15 mK. The two sensors integrated within the cell at opposite sides of the diameter show differences of less than 10 mK and have an average deviation of somewhat less than 3 mK. When directly attached to the outside of the cell body, the thin film sensors reproduce the temperature within the uncertainty of the sensor calibration. Gradients along the inlet tubing vary and were up to 90 mK for the outermost sensor and about one third of this amount at about 30 mm distance from the cell center. We use the latter value of 30 mK for estimating the uncertainty in the gas temperature, assuming a rectangular probability distribution function. This results in a standard uncertainty of $u(T) = 19$ mK, corresponding to $u_r(T) = 6.6 \cdot 10^{-5}$.

F. Refractivity $\mathcal{R}'$

The molecular refractivity is taken from Birch [12], who provides no direct uncertainty on that value, but states in his Table 2 that $n - 1 = (282.12 \pm 0.05) \cdot 10^{-6}$ at 101325 Pa and 15 °C, where the uncertainty is given at the 99 % level of confidence. We use this value as a conservative estimate to obtain $u_r(\mathcal{R}') = 6.3 \cdot 10^{-5}$.

G. Fundamental physical constants N_A and R:

The standard uncertainties of the Avogadro number (N_A) and the molar gas constant (R) have been inferred from the most recent recommendation by the CODATA group [15]. The corresponding relative standard uncertainties are listed in Table 2.

H. Length *L*:

The combined standard uncertainty of the cell length L is obtained through uncertainty propagation according to Eq. (8) and using entries 2 to 5 in Table 1. In order to do so, the standard uncertainty in the refractive index difference has been calculated using Eq. (12) and entries 6 to 10 in Table 1. During all measurements, the cell temperature is kept at about 21 °C within a ± 0.5 K range. The inox cell has a thermal expansion coefficient of 10^{-5}, making thermal dilatation more than 10 times smaller than our measurement uncertainty. Bending of the cell windows due to the pressure gradient between in and outside of the cell varying from -0.015 to $+0.1$ MPa during a measurement cycle induces a cell length change of about 0.14 µm or less. This is at least three times smaller than the upper limit for the impact of thermal dilatation and both these effects could thus be neglected.

4. RESULTS AND DISCUSSION

The measurements of four days were grouped into corresponding measurement series. The results of the individual series and

the totality of the data are summarized in a boxplot (Fig. 5) and Table 2. The third measurement was done at a slight inclination of the cell axis with respect to the laser beam ($\phi = 2.73°$), giving a light path which is longer than the cell length. The result of the light path length $L/\cos(\phi)$ for that configuration is also displayed in Fig. 5.

Pairwise Student's t-tests at a significance level $\alpha = 0.05$ comparing any two of the measurement series show that there are no significant differences between the sample means obtained for each day. In particular, there was no difference between the zero inclination results and the average of the slightly inclined measurements, even though the uncertainty in the inclination factor $\cos\phi$ is much more elevated in the latter ($1.4 \cdot 10^{-4}$ instead of $4.8 \cdot 10^{-6}$). In order to minimize the impact of this bias, we have consequently excluded this particular data set from analysis and discussion, and combined all $\phi = 0°$ data. Nevertheless, the demonstrated dependence on $\cos\phi$ confirms good control of this particular parameter.

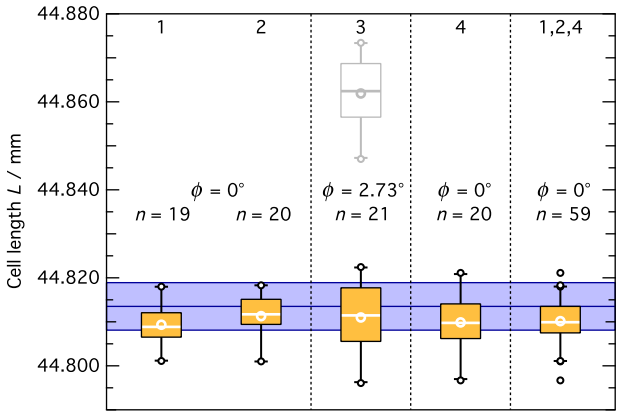

Fig. 5. (Color online) Box-whiskerplot of length measurements performed per day. Whiskers and boxes indicate 5, 25, 75 and 95 percentiles and data beyond the 5 and 95 percentiles are indicated by open circles. Average and median values are shown by white open circles and lines, respectively. The rightmost box summarizes all measurements at $\phi = 0°$. The optical path length of the inclined measurement at day 3 is indicated by the whisker-box in light color. As a reference, the horizontal bar indicates the mechanically derived cell length with its 95 % confidence interval.

The cell length determined from all measurements is $L = 44.810\,\text{mm}$ with an expanded uncertainty of $3.6 \cdot 10^{-4}$ relative or 15 µm absolute. This uncertainty value is based on the uncertainty budget presented in Table 1 and given at the confidence level of 95 % ($k = 2$). All of the 59 data points are within a spread of $+11$ and -14 µm only and the observed relative standard deviation in the measurements is about $1.1 \cdot 10^{-4}$, which essentially corresponds to the uncertainty associated to the fringe number measurement.

The expanded uncertainty of 16 µm covers very well the observed difference of about 4 µm between the interferometrically determined value and the mechanical result (see Fig. 5 and Sec. 2.B). This validates the applicability as well as the reliability of the developed instrument. With the standard uncertainty of $u(L) = 8.0\,\mu\text{m}$, the present interferometer performance has demonstrated an about eightfold improvement as compared to the only other direct short cell measurement [6] we are currently aware of.

In order to further characterize the performance of our instrument, we can consider our interferometer as a refractometer by using the mechanically derived cell length $L = L_m$ and solving Eq. (3) for $n - 1$ instead for L. From the fact that the mechanical measurement is more accurate than our interferometric length, we can conclude that the uncertainty of this refractometer is essentially determined by the Fringe counting uncertainty (see Table 1). We thus find that our instrument is quite close to other state of the art instruments [1, 3] by either considering the relative standard uncertainty of the refractometer of about $4 \cdot 10^{-8}$, or by directly comparing our HeNe fringe resolution of 1/300 to the numbers of 1/400 and 1/600 given for more dedicated instrumentation [7]. Higher refractometer accuracies have so far only been achieved by measuring the modes of a Fabry-Perot cavity [2, 4]. However, this completely different technique is not suitable for absorption cell length measurements.

For a restricted class of absorption cell geometries, direct distance interferometry might provide even more accurate results than our technique. In the direct and areally resolved thickness measurement of opaque gauge blocks, Zhao *et al.* [16] recently obtained sub-micrometer accuracy using low coherence distance measuring interferometry. The method might also be applied to cell length measurements, but it still appears that this requires the refractive index of the window material to be known beforehand, the windows being made from plane parallel plates and the entrance and exit windows also being parallel to each other. In the light of these limitations, our aproach remains the method of choice, even more so as at the demonstrated level of accuracy the absorption cell length is not the limiting factor in quantitative molecular spectroscopy any more.

5. CONCLUSION AND OUTLOOK

We have presented an interferometer for the optical length measurement of an absorption cell. The system works under ambient conditions; the measurement method is contact free and inherently measures the inner dimensions of a gas cell. It can thus be utilized after full assembly of the absorption cell, which therefore avoids some of the drawbacks of a mechanical length measurement. It is shown that the path length measurement of an optical cell at the accuracy level of about 16 µm absolute or a few 10^{-4} relative for few centimeter long cells is possible. This is largely sufficient for performing absorption measurements at the per mil level of accuracy.

The uncertainty budget reveals that the current interferometer performance is limited by the alignment of the interferometer beam through the cell, by the temperature stability and by the fringe number assessment. While the fringe number measurement is likely dominated by acoustic noise and thermal drifts in the interferometer which could be improved in future designs, the temperature stability of the cell, and thus the determination of the refractory index will most probably be the limiting factor in real world absorption measurements, where a temperature accuracy, homogeneity and constancy at the 100 mK level or better may not be reached easily.

The present interferometer design can only be used with cells that can be integrated into the optical path of the setup. A more flexible version of our instrument would involve the use of optical fibers, which allow to locally separate the cell from the remainder of the setup; thus an arbitrary absorption cell could be measured. In the light of the demonstrated performances, a fibered interferometer version might provide a convenient method to determine path lengths with sub-per mil accuracy

Day	Inclination angle / ◦	Average cell length / mm	Standard deviation / µm	Number of repeats	Minimum / mm	Maximum / mm
1	0	44.8093	4.6	20	44.8011	44.8180
2	0	44.8113	4.4	19	44.8010	44.8183
3	2.73	44.8110	7.9	21	44.7961	44.8224
4	0	44.8099	5.5	20	44.7967	44.8211
Ensemble(1, 2, 4)	0	44.8101	4.8	59	44.7967	44.8211

Table 2. Summary statistics of length measurements

also in multi-pass configurations, such as in White or Herriot cells. This is particularly interesting as far as current calibration methods for the determination of path lengths in multi-pass arrangements are still associated with standard uncertainties in the few per mil range [17].

Acknowledgement. The authors gratefully acknowledge the support of H. Fleurbaey from LKB/UPMC, who helped with the calibration of our HeNe laser using the WS7 wavemeter and who performed the reference measurements on the LKB Rb-2 photon frequency standard. Many thanks are also due to S. Pledel from ISIR/UPMC who realized the length measurements employing a high precision linear height gage. H. E and C. J. want to express their gratitude to P. Jeseck for providing a calibrated Vaisala PTB210 barometer for checking the pressure gage performance at ambient pressure. Many thanks go also to J. Viallon from BIPM, who provided very helpful remarks and insightful comments.

REFERENCES

1. N. Khélifa, H. Fang, J. Xu, P. Juncar, and M. Himbert, "Refractometer for tracking changes in the refractive index of air near 780 nm." Appl. Opt. **37**, 156–161 (1998).
2. P. F. Egan and J. A. Stone, "Absolute refractometry of dry gas to ± 3 parts in 10^9," Appl. Opt. **50**, 3076–3086 (2011).
3. P. Huang, J. Zhang, Y. Li, and H. Wei, "Note: Real-time absolute air refractometer." Rev. Sci. Instr. **85**, 056107 (2014).
4. P. F. Egan, J. A. Stone, J. H. Hendricks, J. E. Ricker, G. E. Scace, and G. F. Strouse, "Performance of a dual Fabry-Perot cavity refractometer," Opt. Lett. **40**, 3945–3948 (2015).
5. A. Castrillo, G. Gagliardi, G. Casa, and L. Gianfrani, "Combined interferometric and absorption-spectroscopic technique for determining molecular line strengths: Applications to CO_2," Phys. Rev. A **67**, 062503 (2003).
6. J. Viallon, S. Lee, P. Moussay, K. Tworek, M. Petersen, and R. I. Wielgosz, "Accurate measurements of ozone absorption cross-sections in the Hartley band," Atmos. Meas. Tech. **8**, 1245–1257 (2015).
7. L. R. Pendrill, "Refractometry and gas density," Metrologia **41**, S40–S51 (2004).
8. E. Hedlund and L. R. Pendrill, "Improved determination of the gas flow rate for UHV and leak metrology with laser refractometry," Meas. Sci. Technol. **17**, 2767–2772 (2006).
9. A. Zajac, H. Sadowski, and S. Licht, "Real fringes in the Sagnac and Michelson interferometers," Am. J. Phys. **29**, 669–673 (1961).
10. JCGM/WG 1 2008 Working Group, "Evaluation of measurement data – guide to the expression of uncertainty in measurement," Tech. rep. JCGM 100:2008, BIPM, IEC, IFCC, ILAC, ISO, IUPAC, IUPAP and OIML (2008).
11. P. Juncar, H. Elandaloussi, M. E. Himbert, J. Pinard, and A. Razet, "A new optical wavelength ratio measurement apparatus: the fringe counting sigmameter," IEEE T. Instrum. Meas. **46**, 690–695 (1997).
12. K. P. Birch, "Precise determination of refractometric parameters for atmospheric gases," J. Opt. Soc. Am. A **8**, 647–651 (1991).
13. R. Span, E. W. Lemmon, R. T. Jacobsen, W. Wagner, and A. Yokozeki, "A reference equation of state for the thermodynamic properties of nitrogen for temperatures from 63.151 to 1000 K and pressures to 2200 MPa," J. Phys. Chem. Ref. Data **29**, 1361–1433 (2000).
14. B. de Beauvoir, F. Nez, L. Julien, B. Cagnac, F. Biraben, D. Touahri, L. Hilico, O. Acef, A. Clairon, and J. J. Zondy, "Absolute frequency measurement of the $2S - 8S/D$ transitions in hydrogen and deuterium: New determination of the Rydberg constant," Phys. Res. Lett. **78**, 440–443 (1997).
15. P. J. Mohr, D. B. Newell, and B. N. Taylor, "CODATA Recommended Values of the Fundamental Physical Constants: 2014," ArXiv e-prints (2015).
16. Y. Zhao, G. Schmidt, D. T. Moore, and J. D. Ellis, "Absolute thickness metrology with submicrometer accuracy using a low-coherence distance measuring interferometer," Appl. Opt. **54**, 7693–7700 (2015).
17. J. A. Nwaboh, O. Witzel, A. Pogány, O. Werhahn, and V. Ebert, "Optical path length calibration: A standard approach for use in absorption cell-based IR-spectrometric gas analysis," Int. J. Spectrosc. **2014**, 1–9 (2014).